ADVANCED FUNCTIONAL MATERIALS
www.afm-journal.de

Quaternized Pyridyloxy Phthalocyanines Render Aqueous Electron-Donor Carbon Nanotubes as Unprecedented Supramolecular Materials for Energy Conversion

Eduardo Anaya-Plaza, María Moreno Oliva, Andreas Kunzmann, Carlos Romero-Nieto, Rubén D. Costa, Andrés de la Escosura, Dirk M. Guldi,* and Tomás Torres**

Exploring new properties in known materials, sometimes even achieving behaviors opposite to those traditionally encountered, is a fundamental aspect of innovation in materials science. In the field of energy conversion, for example, the development of water-processed organic solar cells provides environmentally friendlier materials, which contribute to reduce health risks. Herein, a novel approach is described to produce water-soluble electron-donor single wall carbon nanotube (SWCNT) hybrids based on the noncovalent immobilization of quaternized pyridyloxy zinc phthalocyanines (ZnPc) with a varying number of pyridyl substituents. Moreover, the excellent electron-accepting ability of the latter ZnPcs is reported. The introduction of *tert*-butylphenyl groups at the pyridines enables for the first time a complete characterization. The electron-acceptor nature of the ZnPcs enables switching the role of SWCNTs within the resulting supramolecular hybrids. Finally, a proof-of-concept demonstration of the SWCNT/ZnPc hybrids' capacity for energy conversion is presented, paving their way to possible use as active layer material in solar cells processed entirely from aqueous solutions.

1. Introduction

A fundamental aspect of innovation in materials science relates to the exploration of new properties in known materials, sometimes even achieving behaviors that are opposite to those traditionally encountered, which expands the scope of the corresponding research areas. In the field of energy conversion the development of organic photovoltaic materials processed from aqueous solution would, for example, reduce health risks and results in environmentally friendlier devices.[1,2] Hydrophilic photoactive building blocks featuring either electron-donating or electron-accepting characteristics have been much less studied than their hydrophobic analogs.[3] Taking photovoltaic components into aqueous media should bring new capacities of those components. Recently, some of us reported on solar cells integrating hydrophilic phthalocyanines (Pc) bearing negatively charged sulfonated functionalities.[4] These devices were not entirely processed from aqueous solution, owing to the fact that the electron acceptor layer was an evaporated thin film of C_{60}. Herein, we extend this approach to an entirely water-soluble system through the noncovalent immobilization of cationic zinc phthalocyanines (ZnPc) **1** and **2** onto CoMoCAT single wall carbon nanotubes (SWCNT) – **Figure 1**. Such strategy affords water-soluble, hydrophilic photosynthetic reaction centers – SWCNT/ZnPc – in which ZnPc acts as electron-acceptor and SWCNT serves as electron-donor. The latter contrasts with the commonly encountered functions, in which ZnPc and SWCNT play the role of electron donor and electron acceptor, respectively. The novel SWCNT/ZnPc hybrids were probed as active materials for photovoltaic applications.

Pcs are unique electron-donors due to their high thermal and photostability, and because of their intense absorption in the red/near-infrared (NIR) region of the solar spectrum with extinction values as high as 2×10^5 M^{-1} cm^{-1}.[5–11] Such remarkable features render Pcs excellent antennas that, on one hand, harvest light and, on the other hand, transfer the absorbed energy, in the form of energy or electrons, to suitable acceptors. To date, a number of hydrophobic Pcs have been implemented into artificial photosynthetic systems in combination with different carbon nanostructures as electron-accepting materials, giving rise to long-lived charge-separated states.[6] On the contrary, Pcs with electron accepting character are rather scarce.[12] For this purpose, they need to bear highly electron-withdrawing substituents.[13–17]

SWCNTs are considered key materials in nanotechnology as a result of their nanometer-scale size and their extraordinary chemical, mechanical, thermal, and electronic properties.[18–23]

E. Anaya-Plaza, Dr. A. de la Escosura, Prof. T. Torres
Departamento de Química Orgánica (C-I)
Universidad Autónoma de Madrid/IMDEA Nanociencia (TT)
Cantoblanco, 28049 Madrid, Spain
E-mail: andres.delaescosura@uam.es; tomas.torres@uam.es

Dr. M. M. Oliva, A. Kunzmann, Dr. C. Romero-Nieto, Dr. R. D. Costa, Prof. D. M. Guldi
Department of Chemistry and Pharmacy and Interdisciplinary Center for Molecular Materials
Friedrich Alexander-Universität Erlangen-Nürnberg
91058 Erlangen, Germany
E-mail: dirk.guldi@fau.de

DOI: 10.1002/adfm.201503002

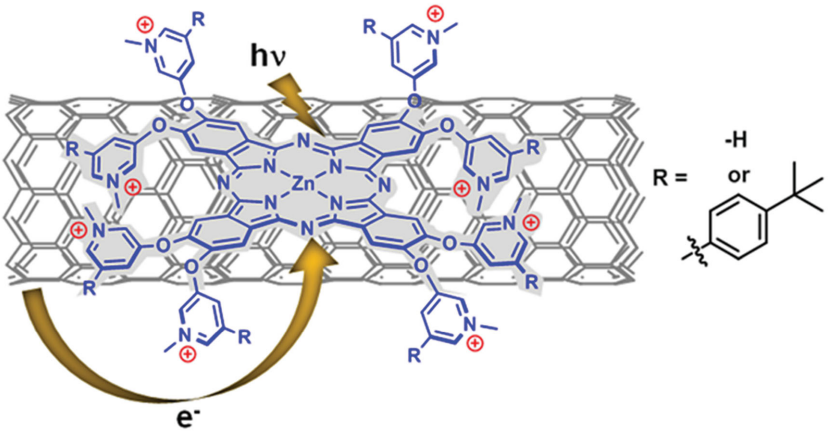

Figure 1. Schematic representation of the described aqueous SWCNT/ZnPc supramolecular hybrids.

A number of covalent[24] and noncovalent[25,26] strategies have been developed in recent years to functionalize SWCNTs with photoactive units, which upon photoexcitation give rise to intramolecular energy and electron transfer events. Noncovalent methodologies do not affect the electronic structure of SWCNTs and are simpler from a synthetic point of view. Any of such strategies to decorate SWCNTs with Pcs afford SWCNT/Pc conjugates and/or hybrids, in which the Pcs normally function as electron donating materials.[27,28] The role of SWCNTs in terms of electron accepting versus electron donating is however exchangeable. Up to now, electron donor SWCNTs were only realized when confronted with strong electron-acceptors such as fullerenes and perylenes.[29,30]

Taking the aforementioned into account, ZnPcs with hydrophilic and strongly electron-withdrawing peripheral substituents are required to guarantee solubility in aqueous media and to invert electron transfer performance of SWCNTs. Achieving water-soluble Pcs constitutes a demanding synthetic challenge. Pcs that are symmetrically substituted with eight quaternizable pyridyloxy substituents, for example, are highly insoluble in most solvents,[31] rendering not only their preparation but also their spectroscopic characterization nearly impossible. On the same note, asymmetric Pcs containing those substituents are unknown, despite the fact that tailoring the number of pyridyloxy moieties at the Pc ring would be a useful approach to tune the Pc features.

In light of the above limitations, a novel series of cationic ZnPcs **2–5** with quaternized 5-(4-*tert*-buthylphenyl)-3-pyridyloxy peripheral substituents was designed and synthesized from their nonquaternized precursors **6–9** (**Figure 2**). The introduction of *tert*-butylphenyl groups is key in terms of balancing hydrophilicity and hydrophobicity, especially for their chromatographic purification, and their chemical as well as physicochemical characterization. Most importantly, we discovered that increasing the number of pyridyloxy substituents in **2–5** gradually increases their electron-accepting nature, yielding first reduction potentials comparable to those of fullerenes (–1.09 V versus Fc/Fc^+) and fullerene derivatives (–1.17 V versus Fc/Fc^+).[32] Two of the ZnPcs, the symmetrical ones (**1** and **2**), were probed as dispersants for CoMoCAT SWCNTs in aqueous media. We reasoned this choice based on the strength of their electron-accepting character. In the resulting CoMoCAT SWCNT/**1** and CoMoCAT SWCNT/**2** hybrids, we demonstrated an electron transfer from SWCNT to ZnPc upon photoexcitation. The latter and the unique stability of CoMoCAT SWCNT/**1** and CoMoCAT SWCNT/**2** encouraged us to integrate them into solar energy conversion schemes.

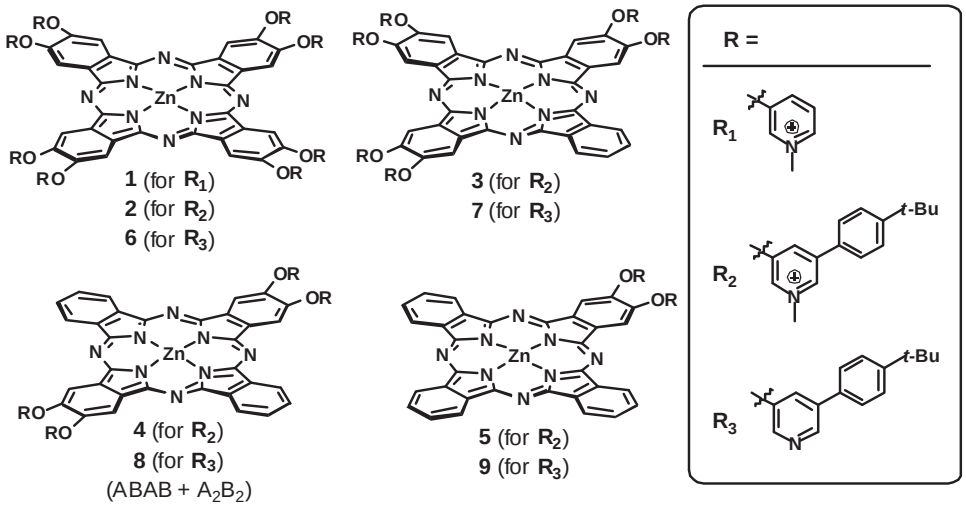

Figure 2. Structure of quaternized and nonquaternized pyridyloxy ZnPc compounds **1–5** and **6–9**, respectively. In the quaternized ZnPc structures, four (for **1** and **2**), three (for **3**), two (for **4**), and one (for **5**) sulfates are the counter ions. The tetrasubstituted derivatives **4** and **8** exist as a mixture of the ABAB and A_2B_2 regioisomers.

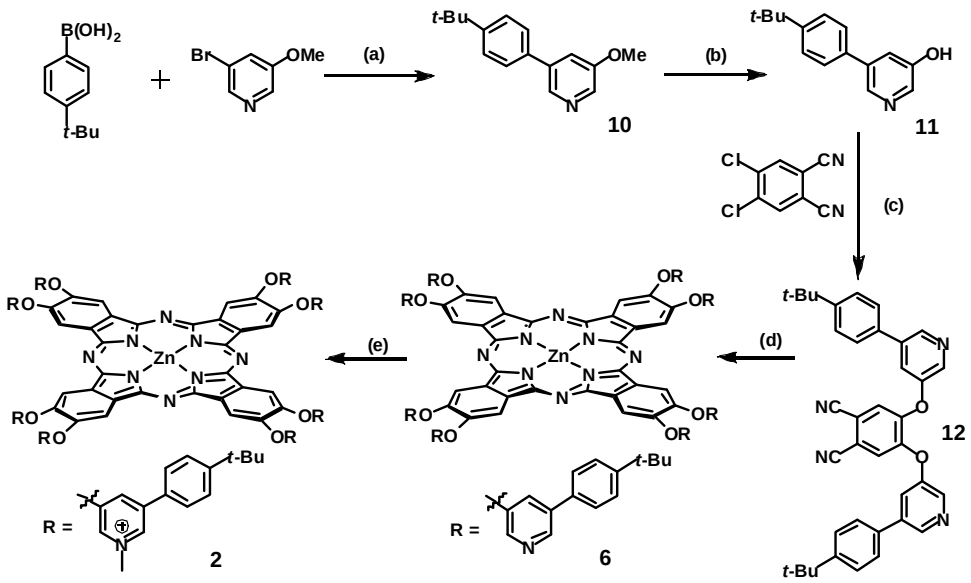

Scheme 1. Synthesis of the quaternized pyridyloxy ZnPc **2**, with four sulfates as counter ions. Conditions and yields: a) $Pd(PPh_3)_4$, 1% aqueous K_2CO_3, DME, 90 °C, 6 h, 90%. b) BBr_3 (1 M in DCM), DCM, 0 °C → rt, 24 h, 84%. c) Anhydrous K_2CO_3, DMF, microwave (200 W, 125 °C, 30 min), 76%. d) $Zn(OAc)_2$, DMAE, 140 °C, 12 h, 66%. e) Me_2SO_4, DMF, 120 °C, 12 h, 80%.

2. Results and Discussion

2.1. Synthesis of Cationic ZnPc Derivatives

Octacationic ZnPc **1** was obtained by adapting a procedure described in the literature.[31] The synthesis of ZnPcs **2–9** – all containing *tert*-butylphenyl groups – started with a Suzuki cross-coupling between 4-*tert*-butylphenylborane and 3-bromo-5-methoxypyridine to yield **10** – **Scheme 1**. Subsequent deprotection of the methoxy groups in **10** with boron tribromide led to 5-(4-*tert*-butylphenyl)pyridin-3-ol (**11**). Phthalonitrile **12** was then obtained by nucleophilic aromatic displacement of the chlorine atoms from 1,2-dichlorophthalonitrile with alcohol **11**. The reaction took place in a microwave reactor, a methodology that improves yields and facilitates the purification process. Phthalonitrile **12** was subsequently reacted overnight with anhydrous zinc acetate in dimethylaminoethanol (DMAE) at 140 °C. The reaction mixture was poured into water/methanol (v/v 1:1), leading upon purification to ZnPc **6** as a green precipitate. Finally, methylation of the peripheral pyridine moieties was carried out in N,N-dimethylformamide (DMF) with dimethyl sulfate at 120 °C, giving rise to ZnPc **2** in 68% yield.

Phthalonitrile **12** is also a precursor for the asymmetrically substituted ZnPcs **3–5** – **Scheme 2**. First, the crossed cyclotetramerization of **12** and 1,2-dicyanobenzene in a 1:1 ratio at 140 °C, with anhydrous $Zn(OAc)_2$ as central metal salt and DMAE as solvent, resulted in a statistical mixture of **6–9**. The latter were separated through column chromatography, using a gradient of toluene/1,4-dioxane (from 5:1 to 2:1, with 1% pyridine) as eluent, from which ZnPcs **6**, **7**, **8** (as a mixture of the ABAB and A_2B_2 regioisomers) and **9** could be isolated. The role of pyridine was to prevent aggregation and to avoid protonation of the Pc pyridyloxy substituents within the column. In the last step, quaternization of ZnPcs **7–9**, under similar conditions as described above, yielded the cationic ZnPcs **3–5** in good yields.

Compounds **2–9** were characterized by nuclear magnetic resonance (NMR), mass spectrometry (MS), infrared, and UV–vis spectroscopy (see the Experimental Section and Supporting Information).

2.2. Electrochemical and Spectroscopic Studies

Absorption spectra of pyridyloxy ZnPcs **6–9** in tetrahydrofuran (THF) reveal a rather sharp Q-band absorption in the range from 670 to 675 nm (Figure S1a, left, Supporting Information), which is a characteristic of monomeric Pcs.[33] In addition, the behavior of the cationic ZnPcs **1–5** was probed in aqueous media. **1** is water-soluble and shows a sharp Q-band at 675 nm (Figure S1a, right, Supporting Information), which again is an indication for the absence of aggregation. The latter stems from electrostatic repulsions between the cationic charges on ZnPc. In stark contrast, **2–5** are insoluble in water, although they dissolve readily in organic solvents such as THF, chloroform, dichloromethane, DMF, dimethyl sulfoxide (DMSO), and methanol.

Dispersing **2–5** in aqueous media, however, is possible by quickly injecting a concentrated methanolic solution into water, reaching a final concentration of 10% methanol and up to 10^{-3} M of the corresponding ZnPcs. As a matter of fact, the resulting dispersions are stable over an extended period of time. From the absorption spectra, which feature a 635 nm absorption band, we derive that ZnPcs **2–5** form H-type aggregates under such conditions.[33] The aggregation extent of these ZnPcs, as revealed by the relative absorption intensities at 635 and 675 nm, depends on the number of peripheral substituents (Figure S1a, right, Supporting Information). Their overall solubility properties, either as monomers or as aggregates, thus relate to the presence of *tert*-butylphenyl groups, which provide a subtle balance between hydrophilicity and hydrophobicity.

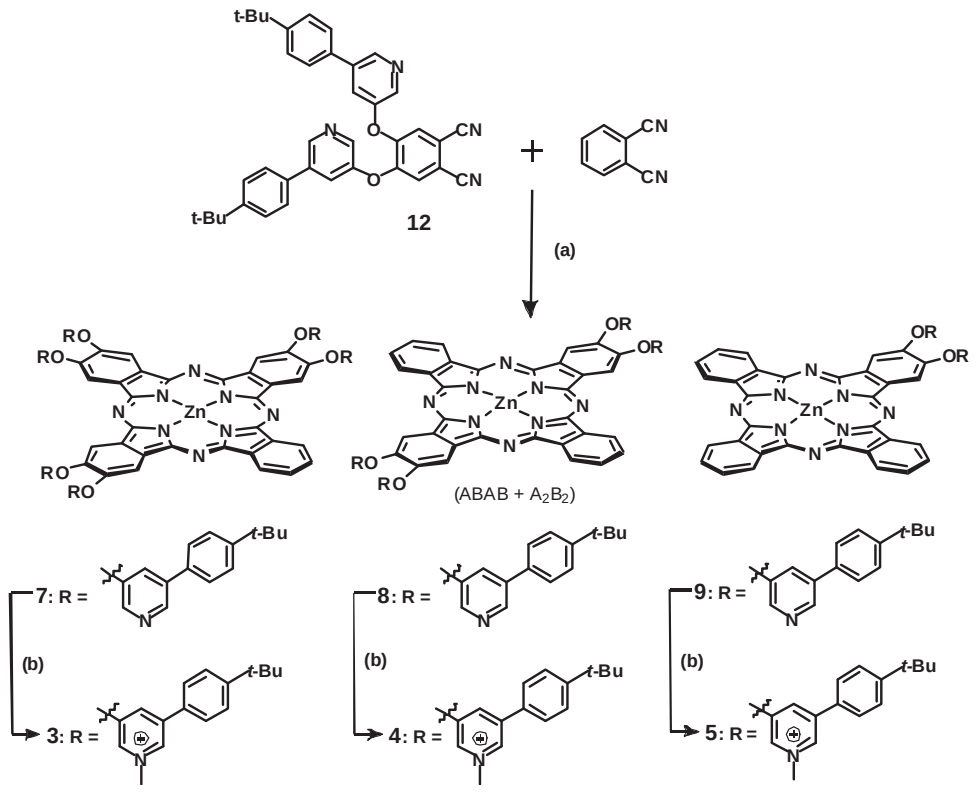

Scheme 2. Synthesis of the quaternized pyridyloxy ZnPcs **3**–**5**, with three (for **3**), two (for **4**), and one (for **5**) sulfates as the counter ions. Compounds **4** and **8** exist as a mixture of the ABAB and A_2B_2 regioisomers. Conditions and yields: a) $Zn(OAc)_2$, DMAE, 140 °C, 12 h. b) Me_2SO_4, DMF, 120 °C, 12 h.

To characterize the electron-accepting nature of ZnPcs with pyridyloxy peripheral substituents, electrochemical studies using cyclic voltammetry (CV) and Osteryoung square wave voltammetry (OSWV) were conducted for **2**–**5** and nonquaternized **6**–**9**. Here, the well-studied tetra-*tert*-butyl-ZnPc (**TT0**) was used as a reference.[34] Notably, neither the electrochemical features of ZnPc **1** nor that of its precursor could be tested due to their lack of solubility in solvents commonly employed for these techniques. For **2**–**5** and **6**–**9**, the redox potentials could be characterized owing to their better solubility as a consequence of having *tert*-butylphenyl groups in the pyridyloxy substituents, and are presented in **Table 1** with the corresponding voltammograms shown in Figure S2 (Supporting Information).

From the voltammograms of **6**–**9** in THF (Figure S2a, Supporting Information), a clear trend as a function of the number of ZnPc pyridyloxy groups is derived. Increasing the number of pyridyloxy groups, for example, results in a slight decrease of the first reduction, that is, from –1.19 V for **9** to –1.14 V for **6**, and a substantial increase of the first oxidation, that is, from +0.29 V for **9** to +0.57 V for **6**, documenting their electron-withdrawing characteristics. This effect is magnified when the pyridyloxy groups are methylated – please compare **2**–**5** in DMSO with **6**–**9** in THF (Table 1 and Figure S2b, Supporting Information).

For **2**–**5**, the irreversible reduction at around –1.6 V increases in intensity as the number of pyridinium groups increases. In other words, the latter groups impact the electrochemical potentials of the Pcs, yet the first reductions could be identified in OSWVs for all the cationic ZnPcs. The corresponding values range from –1.18 V in **5** to –1.02 V in **2** and are in all cases less negative than those observed for the nonquaternized **6**–**9**, indicating the stronger electron accepting nature of the pyridyloxy units once they are quaternized. A similar effect is seen in the anodic scans, with first oxidations ranging from +0.31 V in **5** to +0.65 V in **2** as the number of cationic substituents increases. In sum, incorporating *tert*-butylphenyl groups in **2**–**5** is key to document, for the first time, that quaternized pyridyloxy ZnPcs are excellent electron-acceptors. Moreover, symmetrically substituted ZnPcs **1** and **2** are by far the best electron-acceptors within the whole series. They were therefore chosen as the main target compounds to be immobilized onto SWCNTs, for which the following studies were focused on their full photophysical characterization.

To investigate interactions with SWCNTs, we first prepared and characterized solutions of **1** and **2** in D_2O and in D_2O/methanol (9:1 v/v), respectively, ensuring the formation of monomeric species. Both absorption (Figure S1, Supporting Information) and fluorescence (Figure S3, Supporting Information) spectra of **1** and **2** reveal slight blueshifts when compared to reference **TT0**. Fluorescence quantum yields, determined by the gradient method, are 0.30 (**TT0**), 0.25 (**1**), and 0.22 (**2**). Fluorescence lifetimes are 4.1 (**TT0**), 3.6 (**1**), and 3.5 ns (**2**). Notably, the lower fluorescence quantum yields and the faster fluorescence deactivations in **1** and **2** are probably a consequence of their increased molecular size with respect to **TT0**.

Next, we conducted spectroelectrochemistry to establish the ZnPc radical anion signature for **1** and **2** (Figure S4, Supporting Information). For **1**, maxima are seen at 430, 574, and 715 nm, while minima evolve at 359, 610, and 675 nm. For **2**,

Table 1. Electrochemical data for compounds **1**–**9** determined by OSWV.

ZnPc	E_{red3}	E_{red2}	E_{red1}	E_{ox1}	E_{ox2}
1[a)]	–1.50	–	–1.00	0.61	–
2[a)]	–1.53	–1.12	–1.02	0.65	0.83
3[a)]	–1.47	–1.26	–1.07	0.53	–
4[a)]	–1.49	–	–1.13	0.41	–
5[a)]	–1.59	–1.36	–1.18	0.31[b)]	–
TT0[a)]	–1.81	–1.51	–1.32	0.25	0.50
6[c)]	–1.69	–	–1.14	0.57	–
7[c)]	–1.80	–1.48	–1.14	0.38	0.55
8[c)]	–	–1.59	–1.16	0.31	0.48
9[c)]	–1.83	–1.58	–1.19	0.29	0.40

[a)]$TBAPF_6$ 0.1 M in freshly distilled DMSO; [b)]Data extracted from cyclic voltametry (CV); [c)]$TBAPF_6$ 0.1 M in freshly distilled THF.

the corresponding maxima and minima are found at 433, 577, 740 nm and 360, 612, 678 nm, respectively.

Finally, transient absorption spectroscopy was performed to identify the ZnPc singlet and triplet excited state signatures and their corresponding lifetimes. Photoexcitation at 387 nm leads to the instantaneous formation of the ZnPc singlet excited state. Maxima at 446 and 795 nm, and minima at 608 and 677 nm, are noted for **1** (Figure S4b, left, Supporting Information), while maxima at 446 and 798 nm as well as minima at 637 and 680 nm evolve for **2** (Figure S4b, right, Supporting Information). The singlet-excited states are metastable and start to slowly decay on the picosecond time scale. When turning to the time profiles at 800 nm, lifetimes of 2.2 ns for **1** and of 3.9 ns for **2** reflect the intersystem crossing of the singlet excited state to the triplet manifold.

2.3. Noncovalent Immobilization of ZnPcs 1 and 2 onto SWCNTs

Key toward testing interactions in CoMoCAT SWCNT/ZnPc hybrids is the preparation of suspensions from CoMoCAT SWCNTs in D_2O or D_2O/MeOH (9:1 v/v). The latter were prepared following our previously described procedures.[35,36] In particular, we titrated the SWCNT suspensions with **1** and **2**. In both cases, interactions with CoMoCAT SWCNTs are discernible. For example, in the visible region, the ZnPc Q-band absorptions shift from 673 to 690 nm for **1**, and from 677 to 692 nm for **2** (**Figure 3**a). In the NIR region, the CoMoCAT SWCNT absorptions also reveal a redshift.

To complement the absorption assays, CoMoCAT SWCNT/ZnPc hybrids were subjected to emission measurements upon excitation in the area from 600 to 800 nm (Figure 3b). The results were compared to CoMoCAT SWCNT suspended with a standard surfactant, that is, sodium dodecylbenzenesulfonate (SDBS), in D_2O. All suspensions were prepared with comparable absorption throughout the excitation area. For CoMoCAT SWCNT/SDBS, emission maxima at 961, 1028, 1125, and 1250 nm were measured, which correspond to SWCNT with chirality (6,5), (7,5), (7,6), and (10,5), respectively.[37] For CoMoCAT SWCNT/ZnPc hybrids, a similar but bathochromically shifted emission pattern was found. Importantly, the emission intensities of CoMoCAT SWCNT/ZnPc are dramatically quenched when compared to CoMoCAT SWCNT/SDBS (Figure S5, Supporting Information). This observation goes hand in hand with an immobilization of **1** and **2** onto CoMoCAT SWCNTs.

Additional insights into structural and electronic characteristics of the hybrids were derived from solid-state Raman experiments with 1064 nm excitation.[38,39] Figure 3c illustrates all the important signatures of CoMoCAT SWCNTs, that is, their radial breathing mode (RBM-), D-, and G-modes, together with the 2D-mode. The D-band in CoMoCAT SWCNT/ZnPc hybrids at 1285 ± 2 cm^{-1}, as the reflection of structural damages in CoMoCAT SWCNTs,[40] increases slightly when compared to CoMoCAT SWCNT/SDBS. Likewise, no changes evolved for the G-band in CoMoCAT SWCNT/ZnPc hybrids. The 2D-mode, in turn, shifts from 2548 ± 2 cm^{-1} for CoMoCAT SWCNT/SDBS to 2555 ± 2 cm^{-1} for CoMoCAT SWCNT/**1** and CoMoCAT SWCNT/**2**. Finally, the RBM-modes reveal also upshifts. Altogether, this indicates that π–π interactions are operative between CoMoCAT SWCNTs and ZnPcs.

Finally, we probed the nature of the excited-state interactions between CoMoCAT SWCNTs and ZnPcs by means of transient absorption measurements. Upon excitation of CoMoCAT SWCNT/SDBS in D_2O at either 387 or 660 nm, the instantaneous bleaching of CoMoCAT SWCNT-centered transitions was noted. These are exact mirror images of the ground state absorption (**Figure 4**a). In particular, bleaching of the CoMoCAT SWCNT van Hove singularities evolves in the form of minima at 1031, 1128, and 1256 nm, as well as a shoulder at 986 nm. Upon photoexciting CoMoCAT SWCNT/**1** and CoMoCAT SWCNT/**2** at 387 nm, spectroscopic and kinetic differences are discernible. In terms of spectroscopy, the ZnPc singlet excited state fingerprints evolve. To this end, the visible range is dominated by transient maxima and minima in the 550 to 700 nm range (Figure S6, Supporting Information). Interestingly, the new maximum at 585 nm correlates well with the one-electron reduced ZnPc, as corroborated in spectroelectrochemical experiments. Another important feature is the minimum around 690 nm, which resembles ZnPc immobilized onto CoMoCAT SWCNTs. In the near-infrared region, minima appear at 1110 and 1204 nm for CoMoCAT SWCNT/**1**, and at 1076 and 1200 nm for CoMoCAT SWCNT/**2**. The redshift of the CoMoCAT SWCNT absorption features indicates the formation of charge transfer product, that is, oxidized CoMoCAT SWCNT and reduced ZnPc. In terms of kinetics, the excited state decay processes for the CoMoCAT SWCNT/ZnPc hybrids are faster, that is, 0.6 and 45 ps for CoMoCAT SWCNT/**1** and 0.5 and 14 ps for CoMoCAT SWCNT/**2**, when compared to 0.9 and 215 ps seen for CoMoCAT SWCNT/SDBS (Figure 4d).

2.4. Photovoltaic Devices

Encouraged by the photophysical behavior of CoMoCAT SWCNT/ZnPc hybrids, the fabrication of SWCNT-based photovoltaic cells processed from aqueous solutions was undertaken. ZnPc **1** was chosen to build our prototype device, since it provides the highest solubility in water. First of all, films of different thicknesses were

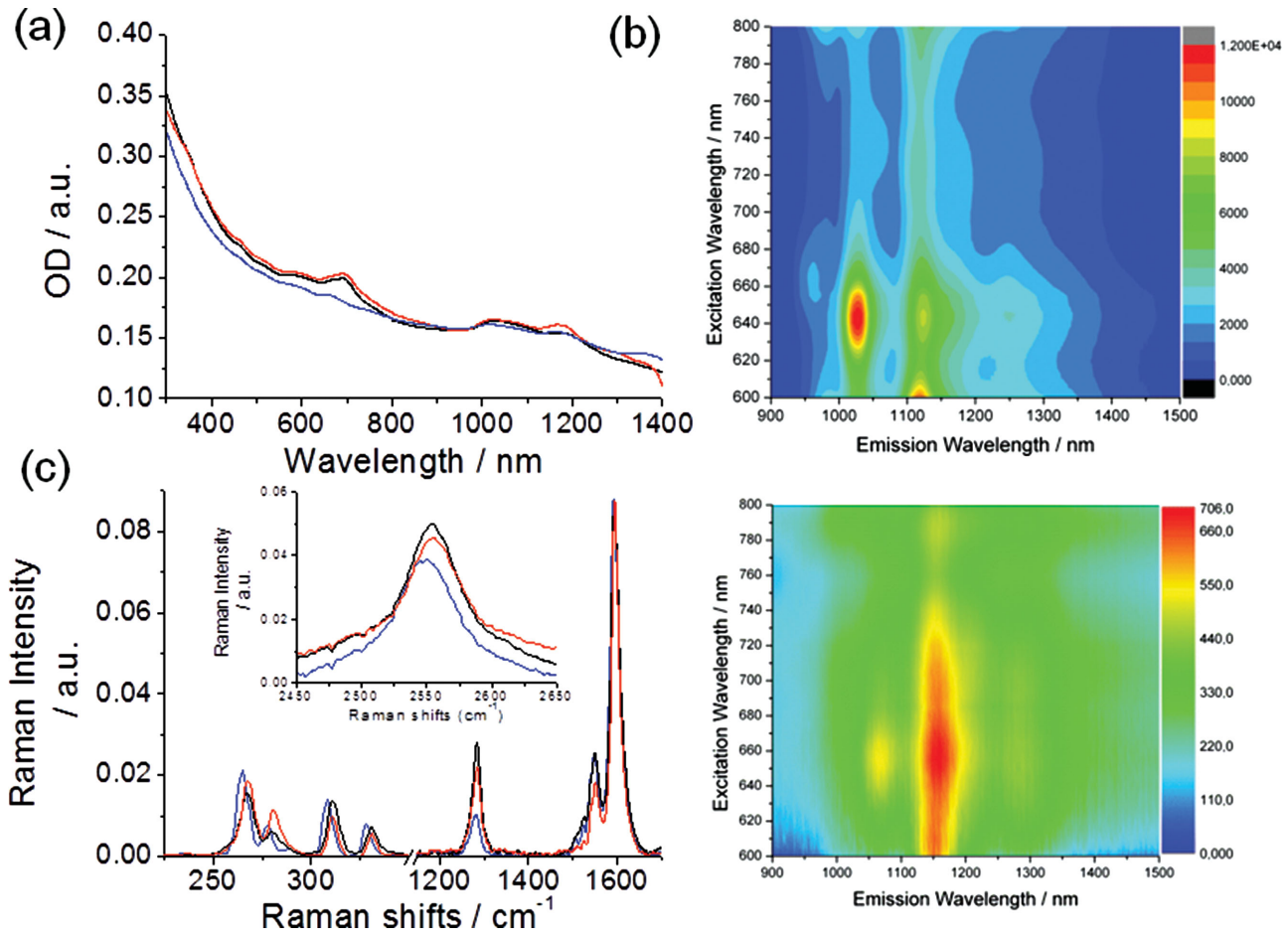

Figure 3. a) Absorption spectra of CoMoCAT SWCNT (dot, black), CoMoCAT SWCNT/**1** (solid, black), and CoMoCAT SWCNT/**2** (solid, gray) suspensions in D_2O and D_2O/MeOH (10%), respectively. b) Steady-state 3D NIR fluorescence spectra of CoMoCAT SWCNT/SDBS (top) and CoMoCAT SWCNT/**1** (bottom) in D_2O, with increasing intensity from gray to black. c) FT-Raman spectra of CoMoCAT SWCNT (dot, black), CoMoCAT SWCNT/**1** (solid, black), and CoMoCAT SWCNT/**2** (solid, gray) in the solid state – 1064 nm excitation. A color version is included at the end of the Supporting Information.

prepared by spraying varying amounts of a CoMoCAT SWCNT/**1** D_2O solution on precleaned fluorine-doped tin oxide (FTO) substrates, placed onto a 200 °C heating plate. The resulting photoelectrodes were probed by absorption spectroscopy, four-point probe resistivity measurements, and profilometry. The latter is an alpha-step technique to monitor both the film thickness and roughness upon spray deposition. Importantly, the use of the spray pyrolysis technique enables homogeneous film formation (**Figure 5**a). Scanning electron microscopy (SEM) images, for example, corroborate that the FTO surface is completely covered by a homogeneous film, where the structure of SWCNTs is preserved (Figure 5b). Moreover, the film thickness could be easily controlled by spraying different amounts of the initial solution, as confirmed by both absorption spectroscopy and profilometry. For example, the absorption features at 650–700 nm, related to the presence of **1** in the hybrid, rise in intensity from 0.3 to 0.6 and to 1.0 when increasing the film thickness from 90 to 250 and 700 nm, respectively. Accordingly, the bulk electrical resistance of the films also increases with thickness, featuring 9–18 $\Omega\ \square^{-1}$ values, which are close to that of bare FTO (Figure S7, Supporting Information).

Such characteristics underline the potential of CoMoCAT SWCNT/**1** hybrid films as novel photoelectrodes for solar energy conversion. The devices were completed by using an equimolar 3 M Na_2S/S/NaOH electrolyte and a Cu_2S-based counter-electrode (see the Supporting Information for more details). Figure 5c shows the photocurrent generated under one sun illumination at AM 1.5 conditions by devices with photoelectrodes featuring different thicknesses. Table S1 (Supporting Information) summarizes the device characteristics. Overall, these results reveal a great potential to prepare fully water-processed solar cells. The increase of the film thickness up to 250 nm leads to an enhancement of the photocurrent density (J) to 0.369 mA cm^{-2} owing to the right balance between high absorption intensity and low bulk electrical resistivity of the photoanodes – vide supra. In stark contrast, devices with a thickness of up to 700 nm show a significant reduction of J with values of 0.228 mA cm^{-2}. This drop in J relates quite likely to the high bulk electrical resistivity and, in turn, hampers the charge collection due to efficient electron recombination processes across the film/electrolyte interface. Open-circuit voltages (V_{oc}) seem to continuously decrease from

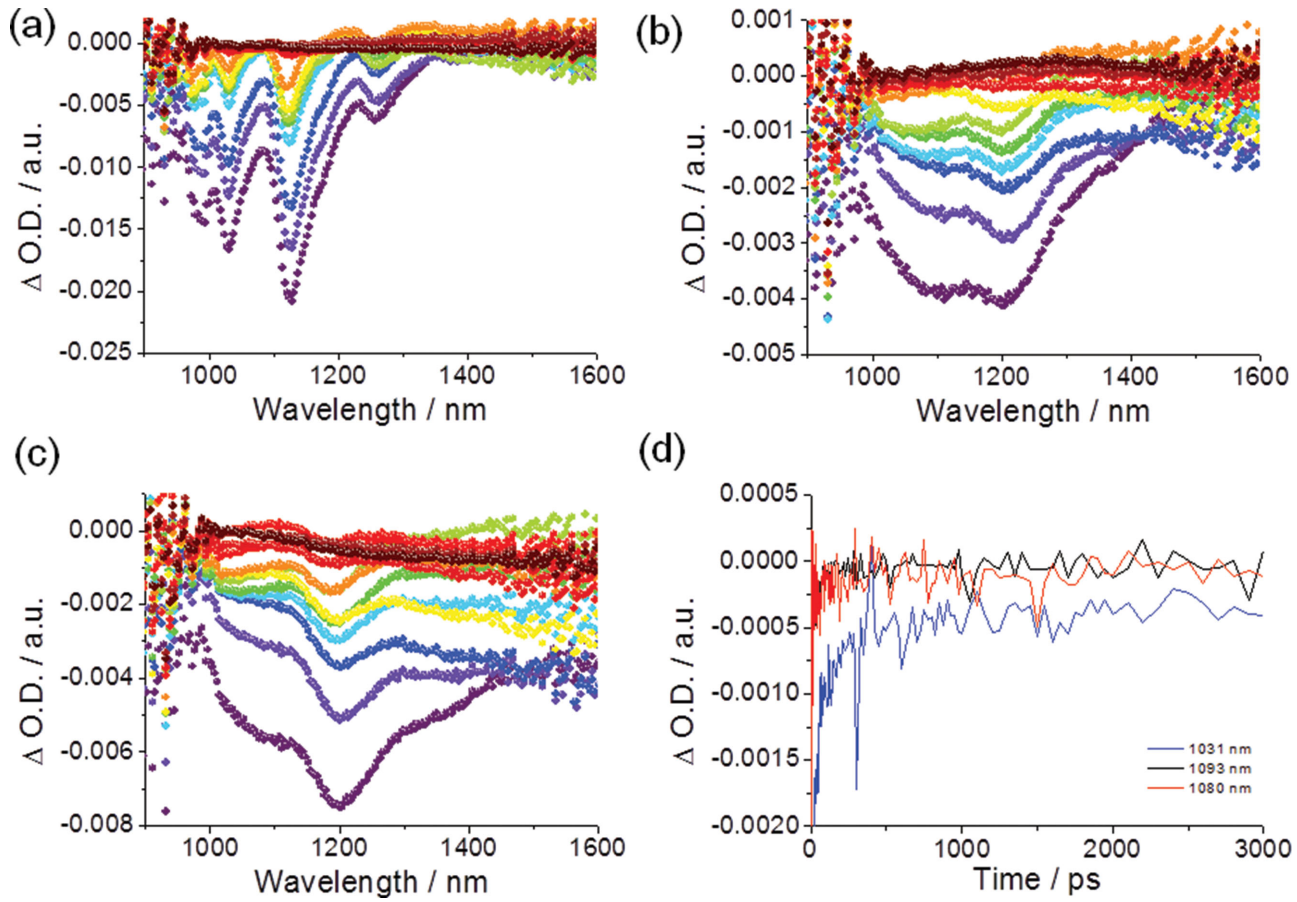

Figure 4. Differential absorption spectra (extended NIR) obtained upon femtosecond pump probe experiments (387 nm) of a) CoMoCAT SWCNT/SDBS, b) CoMoCAT SWCNT/**1**, and c) CoMoCAT SWCNT/**2** in D_2O and D_2O/MeOH, respectively, with several time delays between 1 and 7500 ps, at room temperature. d) Time absorption profiles obtained upon femtosecond pump probe experiments (387 nm) of CoMoCAT SWCNT (blue), CoMoCAT SWCNT/**1** (black), and CoMoCAT SWCNT/**2** (red) in D_2O and D_2O/MeOH (10%), respectively. A color version is included at the end of the Supporting Information.

46 to 16 mV upon increasing the film thickness. As a consequence, the device with a 250 nm photoanode shows the best performance. Importantly, the incident photon-to-current efficiency (IPCE) spectrum resembles the absorption features of **1**, showing maxima of 0.6% and 0.25% at the Soret- and Q-band wavelengths, respectively (Figure 5d). This result is in perfect agreement with the solution based photophysical data – an efficient charge separation sets in only when ZnPcs are excited. The fact that energy conversion is restricted to photons absorbed by ZnPc limits their efficiency, but leaves much room for improvement through the use of additional and complementary photoactive layers in tandem solar cells.

3. Conclusion

In summary, a novel approach is presented toward the production of water-soluble electron donor–acceptor hybrids featuring SWCNTs and ZnPcs as electron donors and electron acceptors, respectively. Such a combination of properties is unprecedented for ensembles made of these two photoactive components. Key to our strategy was the immobilization of quaternized pyridyloxy ZnPcs onto CoMoCAT SWCNTs. To this end, a series of ZnPcs bearing a variable number of quaternized pyridyloxy groups was prepared and purified for the first time as a result of placing *tert*-butylphenyl substituents at the 5-position of the pyridine moieties. Electrochemical assays confirmed the strong electron accepting ability of the ZnPcs, which is comparable to those of the best electron acceptors. Compared to conventional ZnPcs, which act as electron donors when interfaced with SWCNTs, our novel ZnPcs enable a reversed charge transfer in the resulting water-soluble electron donor–acceptor hybrids, namely, from the electron donating SWCNTs to the electron accepting ZnPcs. In proof-of-concept experiments, the obtained SWCNT/ZnPc hybrids have been used for energy conversion in photovoltaic devices, opening the way toward solar cells entirely processable from aqueous solutions.

4. Experimental Section

Synthesis – General Considerations: All reagents were used as purchased from commercial sources (Sigma Aldrich) without further purification. CoMoCAT SWCNT were purchased from Sigma Aldrich, and were produced by a CoMoCAT catalytic chemical vapor deposition (CVD) process, using a flow of pure carbon monoxide (CO) at a pressure of 1^{-10} atm. The nanotubes are grown by CO disproportionation (i.e.,

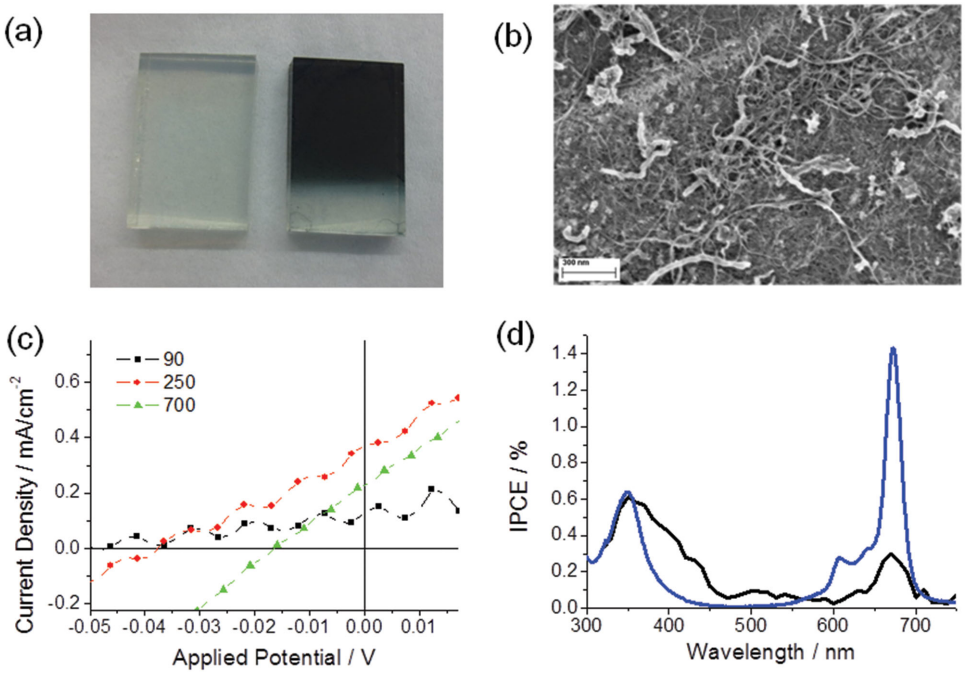

Figure 5. a) Pictures of a FTO substrate (left) and a CoMoCAT SWCNT/**1** thin-film (right) deposited onto FTO substrate by spray pyrolysis. b) SEM image of a CoMoCAT SWCNT/**1** thin-film deposited onto FTO substrate by spray pyrolysis. c) *J–V* curves of devices with CoMoCAT SWCNT/**1** photoelectrodes featuring 90 (black), 250 (red), and 700 nm (green) thickness. d) Photoaction spectrum (in black) of a device with a 250 nm thick CoMoCAT SWCNT/**1** photoelectrode, measured under AM 1.5/1 sun conditions. For comparison purposes, the absorption spectrum of **1** is shown in blue. A color version is included at the end of the Supporting Information.

decomposition into C and CO_2) at 700–950 °C in the presence of a Co-Mo catalyst. Solvents were purchased from Carlo Erba Reagents and dried through standard techniques prior to use. All reactions were performed in standard glassware, under inert argon atmosphere when indicated. Microwave reactions were carried out in a CEM Discovery monomode reactor. Reactions were monitored by thin-layer chromatography (TLC) using TLC plates precoated with silica gel 60F254 (Merck). Column chromatography was carried out on Merck's silica gel 60, 40–63 µm (230–400 mesh). Melting points were recorded in a Stuart Melting Point SMP3 apparatus. ^{1}H and ^{13}C NMR spectra were recorded using Bruker AC-300 (300 MHz) instruments, and the solvent signal was used for internal calibration. UV–vis spectra were recorded with a JASCO V-660 spectrophotometer. Matrix-assisted laser desorption/ionization - time of flight (MALDI-TOF) and electrospray ionization (ESI) mass spectra were recorded with a Bruker Ultrareflex III spectrometer and with an Applied Biosystems QSTAR using an injection system HPLC1100 (Agilent Technologies), respectively.

Octakis(1-methyl-3-pyridiniumoxy)-ZnPc, tetrasulfate (***1***): It was synthesized by adapting a procedure previously reported.[31]

Octakis(5-tert-butylphenyl-1-methyl-3-pyridiniumoxy)-ZnPc, tetrasulfate (***2***): Into a 50 mL two-neck round-bottom flask, compound **6** (95.3 mg, 0.04 mmol) was dissolved in 5 mL of anhydrous DMF and warmed up to 120 °C. Dimethyl sulfate (0.1 mL, 1.1 mmol) was then added. After 24 h, 10 mL of water was added and the solvent was dried under vacuum. The green solid was solubilized in the minimum amount of hot methanol, precipitated with water, and isolated by centrifugation (93.2 mg, 80%). Mp >250 °C; ^{1}H NMR (300 MHz, DMSO-d_6, δ): 9.53 (s, 8H, ZnPc H), 9.27 (s, 8H, Py H), 9.23 (s, 8H, Py H), 8.88 (s, 8H, Py H), 7.79 (d, J = 8.0 Hz, 16H, Ar H), 7.50 (d, J = 8.0 Hz, 16H, Ar H), 4.40 (s, 24H; CH_3), 1.25 (s, 56H; $C(CH_3)_3$); UV–vis (methanol/water (1:9)): λ_{max} (ε) = 677 (69 200), 640 (33 900), 335 nm (63 100).

General Procedure for the Quaternization of Asymmetrically Substituted ZnPcs: Into a 50 mL two-neck round-bottom flask, the corresponding ZnPc was dissolved in 5 mL of anhydrous DMF and warmed up to 120 °C. Dimethylsulfate (30 eq.) was then added. After 24 h, 10 mL of water was added and the solvent was dried under vacuum. The resulting solid residue was dissolved in hot methanol and precipitated with water. The green precipitate was isolated by centrifugation.

Hexakis(5-tert-butylphenyl-1-methyl-3-pyridiniumoxy)-ZnPc, trisulfate (***3***): **7** (103.2 mg, 0.053 mmol) was used as the starting material. Yield: 64%, 78.3 mg. Mp >250 °C; ^{1}H NMR (300 MHz, DMSO-d_6, δ): 9.55 (s, 6H, Py H), 9.40 (s, 2H, ZnPc H), 9.30 (s, 6H, Py H), 9.27 (s, 6H, ZnPc H), 8.97 (s, 3H, Py H), 8.90 (s, 3H, Py H), 8.28 (m, 2H, ZnPc H), 7.83 (m, 12H, Ar H), 7.54 (m, 12H, Ar H), 4.44 (s, 6H; CH_3), 4.41(s, 12H; CH_3), 1.27 (s, 54H; $C(CH_3)_3$); UV–vis (methanol/water (1:9)): λ_{max} (ε) = 682 (52 500), 634 (43 700), 336 nm (69 200).

Tetrakis(5-tert-butylphenyl-1-methyl-3-pyridiniumoxy)-ZnPc, disulfate (***4***): **8** (78.2 mg, 0.053 mmol) was used as the starting material. Yield: 38%, 35.0 mg. Mp >250 °C; ^{1}H NMR (300 MHz, DMSO-d_6, δ): 9.26 (m, 12H, Py H), 8.95 (s, 2H, ZnPc H), 8.85 (s, 1H, ZnPc H), 8.26 (s, 3H, ZnPc H), 7.81 (m, 18H, Ar H), 7.55 (m, 12H, Ar H), 4.44 (m, 12H; CH_3), 1.27 (m, 36H; $C(CH_3)_3$); UV–vis (methanol/water (1:9)): λ_{max} (ε) = 681 (42 700), 637 (33 900), 329 nm (57 500).

Bis(5-tert-butylphenyl-1-methyl-3-pyridiniumoxy)-ZnPc, sulfate (***5***): **9** (16.8 mg, 0.016 mmol) was used as the starting material. Yield: 64%, 11.9 mg. Mp >250 °C; ^{1}H NMR (300 MHz, DMSO-d_6, δ): 9.48 (m, 6H, ZnPc H), 9.37 (m, 2H, ZnPc H), 9.34 (s, 2H, ZnPc H), 9.28 (s, 2H, Py H), 8.96 (s, 2H, Py H), 8.27 (m, 6H, Ar H), 7.83 (d, 4H, J = 8.5 Hz; Ar H), 7.54 (d, 4H, J = 8.5 Hz; Ar H), 4.45 (s, 6H; CH_3), 1.27 (s, 18H; $C(CH_3)_3$); UV–vis (methanol/water (1:9)): λ_{max} (ε) = 680 (20 800), 636 (18 100), 331 nm (28 500); ESI$^+$*m/z* (%): 528.18 (100) [M^{2+}].

Octakis(5-tert-butylphenyl-3-pyridyloxy)-ZnPc (***6***): Into a 25 mL round-bottom flask, phthalonitrile **12** (194.4 mg, 0.406 mmol) and $Zn(OAc)_2$ (30.3 mg, 0,165 mmol) were dissolved in 5 mL of DMAE under argon atmosphere and warmed up to 140 °C overnight. The resulting green solution was poured into a mixture water/methanol (1:1), forming a green precipitate that was filtered off through celite and washed with acetone and diethyl ether. This solid was extracted with THF, leading to a green solid product. Yield: 66%, 132.5 mg. Mp >250 °C; ^{1}H-NMR: (300 MHz, $CDCl_3$, 5% TFA, δ): 9.38 (s, 8H, ZnPc H), 8.83 (s, 8H, Py H), 8.73 (s, 8H,

Py H), 8.46 (s, 8H, Py H), 7.53 (m, 32H, Ar H), 1.30 (s, 72H; $C(CH_3)_3$); UV–vis (THF): λ_{max} (ε) = 674 (26 9000), 608 (43 700), 357 nm (102 000); MALDI *m/z* (%): 4759.2 (71) $[2M]^+$, 4534.0 (1) $[2M\text{-}C_{15}H_{16}NO]^+$, 2379.0 (100) $[M^+]$, 2154.9 (1) $[M\text{-}C_{15}H_{16}NO]^+$; HRMS (MALDI) *m/z*: $[M]^+$ calcd. for $C_{152}H_{136}N_{16}O_8Zn$, 2377.0013; found, 2377.0071.

General Procedure for the Synthesis of Asymmetrically Substituted ZnPcs: Into a 25 mL round-bottom flask, phthalonitrile **12** (623.7 mg, 1.08 mmol), 1,2-dicyanobenzene (133.3 mg, 1.04 mmol), and $Zn(OAc)_2$ (156.0 mg, 0.85 mmol) were dissolved in 5 mL of DMAE under argon atmosphere and subsequently warmed up at 140 °C overnight. The reaction mixture was dried under vacuum, dissolved in 5 mL of THF, precipitated in 100 mL of methanol/water (1:1), and filtered over celite. The obtained blue solid was purified by column chromatography using a toluene/dioxane/pyridine (80:19:1) mixture as eluent. Different fractions were collected and further characterized as **9**, **8**, **7**, and **6** in elution order.

Hexakis(5-tert-butylphenyl-3-pyridyloxy)-ZnPc (***7***): Yield: 29%, 201.8 mg. Mp >250 °C; ^{1}H-NMR: (300 MHz, $CDCl_3$, 5% TFA, δ): 9.45 (s, 2H, ZnPc H), 9.38 (s, 2H, ZnPc H), 9.35 (s, 2H, ZnPc H), 9.34 (m, 2H, ZnPc H) 8.83 (m, 6H, Py H), 8.56 (s, 2H, Py H), 8.50 (s, 2H, Py H), 8.47 (s, 2H, Py H), 8.92 (m, 4H, Py H), 8.72 (m, 2H, Py H), 8.27 (s, 2H, ZnPc H), 7.59 (m, 24H, Ar H), 1.32 (s, 18H; $C(CH_3)_3$), 1.31 (s, 18H; $C(CH_3)_3$) 1.30 (s, 18H; $C(CH_3)_3$); UV–vis (THF): λ_{max} (ε) = 672 (282 000), 606 (47 900), 354 nm (117 000); MALDI *m/z* (%): 3859.2 (48) $[2M]^+$, 3408.6 (1) $[2M\text{-}(C_{15}H_{16}NO)_2]^+$, 1928.7 (100) $[M^+]$, 1478.5 (3) $[M\text{-}(C_{15}H_{16}NO)_2]^+$; HRMS (MALDI) *m/z*: $[M]^+$ calcd. for $C_{122}H_{106}N_{14}O_6Zn$, 1926.7706; found, 1926.7711.

Tetrakis(5-tert-butylphenyl-3-pyridyloxy)-ZnPc (***8***): Yield: 18%, 139.6 mg. Mp >250 °C; ^{1}H-NMR: (300 MHz, $CDCl_3$, 5% TFA, δ): 9.43-9.29 (m, 8H, ZnPc H), 8.90 (m, 4H, Py H), 8.82 (m, 4H, Py H), 8.72 (s, 2H, Py H), 8.56 (s, 2H, Py H), 8.29 (m, 4H, ZnPc H), 7.59 (m, 16H, Ar H), 1.31 (m, 36H; $C(CH_3)_3$); UV–vis (THF): λ_{max} (ε) = 670 (209 000), 605 (21 900), 351 nm (64 600); MALDI *m/z* (%): 4437.7 (2) $[3M]^+$, 2958.1 (18) $[2M]^+$, 1478.5 (100) $[M^+]$; HRMS (MALDI) *m/z*: $[M]^+$ calcd. for $C_{92}H_{76}N_{12}O_4Zn$, 1476.5398; found, 1476.5387.

Bis(5-tert-butylphenyl-3-pyridyloxy)-ZnPc (***9***): Yield: 28%, 98.2 mg. Mp >250 °C; ^{1}H-NMR: (300 MHz, $CDCl_3$, 5% TFA, δ): 9.44-9.26 (m, 8H, ZnPc H), 8.92 (m, 2H, Py H), 8.60 (m, 4H, Py H), 8.30 (m, 4H, ZnPc H), 7,88 (s, 2H, Py H), 7.59 (m, 8H, Ar H), 1.32 (s, 18H, $C(CH_3)_3$); UV–vis (THF): λ_{max} (ε) = 669 (132 000), 603 (10 200), 347 nm (37 200); MALDI *m/z* (%): 2056.5 (5) $[2M]^+$, 1026.3 (100) $[M^+]$; HRMS (MALDI) *m/z*: $[M]^+$ calcd. for $C_{62}H_{46}N_{10}O_2Zn$, 1026.3091; found, 1026.3093.

3-(4-tert-butylphenyl)-5-methoxypyridine (***10***): Into a 50 mL two-neck round-bottom flask, equipped with a reflux condenser, 3-bromo-5-methoxypyridine (2.05 g, 10.9 mmol) and 4-(*tert*-butyl)phenylboronic acid (1.90 g, 10.6 mmol) were dissolved in dimethoxyethane under argon atmosphere. Tetrakis(triphenylphosphine)palladium(0) (120 mg, 0.10 mol) was added and the mixture was stirred for 30 min. Previously deoxygenated aqueous K_2CO_3 (5 g in 15 mL) was then added and warmed up at 90 °C for 5 h. After reaction completion, the mixture was dried under vacuum and extracted with diethyl ether and water. The organic phase was separated and the aqueous layer was washed twice more with diethyl ether (2 × 10 mL). The combined organic extracts were dried over anhydrous $MgSO_4$ and dried under vacuum. The resulting yellowish solid was purified through column chromatography column, using hexane/ethyl acetate (8:3) as eluent. Yield: 90%, 2.30 g. Mp 100 °C; ^{1}H-NMR: (300 MHz, $CDCl_3$, δ): 8.47 (d, J = 1.8 Hz, 1H; Py H), 8.28 (d, J = 2.6 Hz, 1H, Py H), 7.52 (d, J = 2.6 Hz, 4H, Ar H), 7.37 (dd, J_1 = 2.6, J_2 = 1.8 Hz, 1H, Py H), 3.91 (s, 3H; CH_3), 1.37 (s, 9H, $C(CH_3)_3$); ^{13}C NMR (76 MHz, $CDCl_3$, δ): 155.8 (C5), 151.5 (C4′), 140.8 (C2), 137.3 (C3), 135.9 (C6), 134.9 (C1′), 127.1 (C2′), 126.2 (C3′), 119.1 (C4), 55.7 ($\underline{C}H_3$), 34.8 ($\underline{C}(CH_3)_3$), 31.4 ($C(\underline{C}H_3)_3$); DEPT-135 (76 MHz, $CDCl_3$): δ (ppm) = 140.7 (C2), 135.80 (C6), 126.9 (C2′), 126.0 (C3′), 119.0 (C4), 55.6 (CH_3), 31.3 ($C(\underline{C}H_3)_3$).

3-(4-tert-butylphenyl)-5-hydroxypyridine (***11***): Into a 50 mL round-bottom flask, compound **10** (1.94 g, 8.05 mmol) was dissolved in 7 mL of dichloromethane under argon atmosphere and was cooled down to –78 °C. A commercial boron tribromide solution (1 M, 15 mL, 15.0 mmol) was added dropwise. When the addition was completed, the temperature was raised to room temperature and was the mixture was left stirring overnight. The reaction was quenched by the addition of saturated $NaHCO_3$. The phases were separated and the aqueous phase was washed with ethyl acetate (3 × 10 mL). The combined organic extracts were dried over anhydrous $MgSO_4$ and dried under vacuum. The dark brown solid obtained was purified by recrystallization from ethanol. Yield: 84%, 1.54 g. Decompose 163–165 °C; ^{1}H-NMR: (300 MHz, DMSO-d_6, δ): 11.5 (s, 1H; OH), 8.68 (s, 1H, Py H), 8.33 (s, 1H, Py H), 8.07 (s, 1H, Py H), 7.73 (d, J = 8.2 Hz, 2H, Ar H), 7.58 (d, J = 8.4 Hz, 2H, Ar H), 1.33 (s, 9H, $C(CH_3)_3$); ^{13}C NMR (76 MHz, DMSO-d_6, δ): 156.02 (C5), 152.33 (C4′), 139.38 (C2), 132.01 (C6), 131.34 (C4), 129.37 (C3), 127.49 (C1′), 126.99 (C3′), 126.14 (C2′), 34.46 ($\underline{C}(CH_3)_3$), 30.93 ($C(\underline{C}H_3)_3$).

4,5-Bis(5-tert-butylphenyl-3-pyridyloxy)phthalonitrile (***12***): Into a 10 mL round-bottom flask, compound **11** (270.6 mg, 1.19 mmol), 4,5-dichlorophthalonitrile (104.8 mg, 0.532 mmol), and anhydrous K_2CO_3 (780 mg, 5.67 mmol) were dissolved into 5 mL of anhydrous DMF. The mixture was reacted in a microwave reactor for 30 min at 125 °C and 100 W. The reaction was followed by TLC using dichloromethane/methanol (20:1) as eluent. The solvent was then evaporated under vacuum, the crude solid was extracted with water/dichloromethane (1:1, 10 mL) and the aqueous phase washed with dichloromethane (2 × 5 mL). The combined organic phases were dried over anhydrous $MgSO_4$ and then dried under vacuum. The resulting yellowish solid was dissolved in the minimum amount of hot chloroform and precipitated over hot ethanol. Yield: 76%, 194 mg. Mp 223–224 °C; ^{1}H-NMR: (300 MHz, DMSO-d_6, δ): 8.70 (d, J = 1.6 Hz, 2H, Py H), 8.41 (d, J = 2.6 Hz, 2H, Py H), 8.17 (s, 2H, Ar H), 7.83 (m, 2H, Py H), 7.61 (d, J = 8.4 Hz, 4H, Ar H), 7.46 (d, J = 8.4 Hz, 4H, Ar H), 1.31 (s, 9H, $C(CH_3)_3$); ^{13}C NMR (76 MHz, DMSO-d_6, δ): 152.2 (C4+C5), 151.1 (C3′), 150.3 (C4″), 143.6 (C6′), 138.8 (C2′), 136.9 (C5′), 133.0 (C1′), 126.9 (C3″), 126.7 (C3+C6), 125.8 (C2″), 122.7 (C4′), 122.3 (CN), 111.9 (C1+C2), 34.3 ($\underline{C}(CH_3)_3$), 30.9 ($C(\underline{C}H_3)_3$); DEPT-135 (76 MHz, $CDCl_3$): δ (ppm) = 143.3 (C6), 138.8 (C2′), 126.6 (C3″), 126.4 (C3+C6), 125.5 (C2″), 122.5 (C4′), 30.7 ($C(\underline{C}H_3)_3$).

Preparation of SWCNT/ZnPc Hybrids: Pc solutions were prepared in D_2O (**1**) and in a mixture of 10% MeOH and 90% D_2O (**2**). The suspensions of CoMoCAT SWCNT/ZnPc hybrids were prepared in D_2O (CoMoCAT SWCNT/**1**) and D_2O/MeOH (CoMoCAT SWCNT/**2**) by means of repeating several cycles, which include vigorous stirring, ultrasounds for 30 min at 20 °C, and ultracentrifugation. This protocol rendered suspensions that were suitably stabile for our spectroscopic studies.

Spectroscopic and Electrochemical Characterization: Absorption spectroscopy was measured on a Cary 5000 (Varian) two-beam spectrometer. Steady-state fluorescence spectra were taken with a FluoroMax3 spectrometer (HORIBA Jobin Yvon) in the visible detection range and with a FluoroLog3 spectrometer (HORIBA Jobin Yvon) with an IGA Symphony (5121 1 µm) detector in the NIR detection range. The experiments were performed at room temperature. Fluorescence quantum yields were determined by the comparative method using the **TT0** reference (ϕ_F = 0.30 in toluene) as standard. Time correlated single photon counting (TCSPC) spectra were taken with a FluoroLog system (HORIBA Jobin Yvon). The sample was excited by a NanoLED-650 (peak wavelength 647 nm) and the signal was detected by a Hamamatsu MCP photomultiplier (type R3809U-50). The time profiles were recorded at 680 nm. Raman spectra were recorded using a Bruker FT Raman RFS 100 system with a liquid N_2 cooled Ge detector upon excitation by a 1064 nm Nd-YAG laser. Femtosecond transient absorption spectroscopy was performed with 387 nm laser pulses (1 kHz, 150 fs pulse width) from an amplified Ti:sapphire laser system (Model CPA2101 from Clark-MXR Inc.), the laser energy being 200 nJ. Electrochemical experiments were carried out with a Metrohm FRA 2 µAutolab Type III potentiostat, in deaerated DMSO containing 0.1 M tetrabutylammonium hexafluorophosphate ($TBAPF_6$) as the supporting electrolyte. A single-compartment, three-electrode cell configuration was used in this work. Glassy carbon (3 mm diameter) or platinum (2 mm diameter) was used as the working electrode, a platinum wire as the counter, and an Ag wire as the reference electrode. All potentials were corrected against Fc/Fc^+

internal reference. Spectroelectrochemical experiments were performed with a home-made setup containing a potentiostat (Metrohm Autolab PGSTAT 101) and Analytik Jena Specord absorption spectrophotometer. The working electrode has been platinum gauze (99.9%, 1024 mesh cm^{-2}, 0.06 mm wire diameter) from ChemPur, a platinum wire was used as counter electrode, and an Ag wire as reference electrode.

Photovoltaic Devices: FTO plates were extensively cleaned, using ultrasonication in subsequent baths of detergent, acetone, and isopropanol for 15 min each, and in an air cleaner/ozone generator for 18 min. The spray pyrolysis method was used to prepare the SWCNT/ZnPc hybrid films on precleaned FTO slides. In detail, a thin film was prepared by spraying a solution of CoMoCAT SWCNT/ZnPc hybrids (D_2O) using N_2 air flow at 2 atm onto a FTO substrate placed on top of a heater at 200 °C. Next, key film properties, such as morphology, thickness, and conductivity, were investigated by using SEM (Zeiss Gemini Ultra 55), profilometry (KLA Tencor Alpha Step D-100 Stylus), and the 4-point-probe technique (Jandel H-L, Keithley 2400), respectively. The solar cells were constructed using the latter films featuring different thicknesses together with equimolar 3 M Na_2S/S/NaOH electrolyte and Cu_2S-based counter-electrode. Photocurrent measurements were carried out under 1 sun and AM 1.5 conditions using a custom made solar simulator including a 350–1000 W adjustable Xe lamp source (LOT) combined with appropriate filters. Current–voltage measurements were measured by using a potentiostat/galvanostat (PGSTAT30N, Autolab equipped with a frequency response analyzer module – FRA) in the range of –0.8 to 0.2 V. IPCE were performed under 1 sun and AM 1.5 conditions with a Newport Solar Simulator system.

Supporting Information

Supporting Information is available from the Wiley Online Library or from the author.

Acknowledgements

E.A.-P. and M.M.O. contributed equally to this work. AdlE holds a Ramón y Cajal contract from the Spanish Ministry of Economy (MINECO). MMO acknowledges financial support from the Marie Curie COFUND program "U-Mobility" by the Universidad de Málaga and the European Community's Seventh Framework Program under Grant Agreement No. 246550. The EAM cluster in the frame of the DFG excellence programs is ackowledged for their support. This work was supported by the EU (GLOBASOL, FP7-ENERGY-2012-J, 309194-2 and SO2S, FP7-PEOPLE-2012-ITN, 316975), the Spanish MINECO (CTQ-2014-52869-P (TT) and CTQ-2014-53673-P (AdlE)), and Comunidad de Madrid (FOTOCARBON, S2013/MIT-2841).

Received: July 20, 2015
Revised: September 23, 2015
Published online: November 27, 2015

[1] S. Hellweg, U. Fischer, M. Scheringer, K. Hungerbuhler, *Green Chem.* **2004**, *6*, 418.
[2] A. M. Ruder, *Ann. N. Y. Acad. Sci.* **2006**, *1076*, 207.
[3] Y. Huang, E. J. Kramer, A. J. Heeger, G. C. Bazan, *Chem. Rev.* **2014**, *114*, 7006.
[4] J. W. Ryan, E. Anaya-Plaza, A. de la Escosura, T. Torres, E. Palomares, *Chem. Commun.* **2012**, *48*, 6094.
[5] C. G. Bezzu, M. Helliwell, J. E. Warren, D. R. Allan, N. B. McKeown, *Science* **2010**, *327*, 1627.
[6] G. Bottari, G. de la Torre, D. M. Guldi, T. Torres, *Chem. Rev.* **2010**, *110*, 6768.
[7] J. Mack, N. Kobayashi, *Chem. Rev.* **2011**, *111*, 281.
[8] V. V. Roznyatovskiy, C.-H. Lee, J. L. Sessler, *Chem. Soc. Rev.* **2013**, *42*, 1921.
[9] *Handbook of Porphyrin Science* (Eds: K. M. Kadish, K. M. Smith, R. Guilard), World Scientific, Singapore **2013**.
[10] D. Luque, A. de la Escosura, J. Snijder, M. Brasch, R. J. Burnley, M. S. T. Koay, J. L. Carrascosa, G. J. L. Wuite, W. H. Roos, A. J. R. Heck, J. J. L. M. Cornelissen, T. Torres, J. R. Caston, *Chem. Sci.* **2014**, *5*, 575.
[11] F. Setaro, M. Brasch, U. Hahn, M. S. Koay, J. J. Cornelissen, A. se la Escosura, T. Torres, *Nano Lett.* **2015**, *15*, 1245.
[12] M.-E. Ragoussi, J.-J. Cid, J.-H. Yum, G. de la Torre, D. Di Censo, M. Grätzel, M. K. Nazeeruddin, T. Torres, *Angew. Chem. Int. Ed.* **2012**, *51*, 4375.
[13] M. V. Martinez-Dias, S. Esperanza, A. de la Escosura, M. Catellani, S. Yunus, S. Luzzati, T. Torres, *Tetrahedron Lett.* **2003**, *44*, 8475.
[14] R. A. Hatton, N. P. Blanchard, V. Stolojan, A. J. Miller, S. R. P. Silva, *Langmuir* **2007**, *23*, 6424.
[15] Q. L. Song, H. B. Yang, Y. Gan, C. Gong, C. M. Li, *J. Am. Chem. Soc.* **2010**, *132*, 4554.
[16] Y. Zhang, P. Ma, P. Zhu, X. Zhang, Y. Gao, D. Qi, Y. Bian, N. Kobayashi, J. Jiang, *J. Mater. Chem.* **2011**, *21*, 6515.
[17] M.-E. Ragoussi, G. Katsukis, A. Roth, J. Malig, G. de la Torre, D. M. Guldi, T. S. Torres, *J. Am. Chem. Soc.* **2014**, *136*, 4593.
[18] S. Reich, C. Thomsen, J. Maultzsch, *Carbon Nanotubes: Basic Concepts and Physical Properties*, Wiley-VCH, Weinheim, Germany **2004**.
[19] V. N. Popov, P. Lambin, *Carbon Nanotubes*, Springer, Dordrecht, Netherlands **2006**.
[20] S. Fukuzumi, T. Kojima, *J. Mater. Chem.* **2008**, *18*, 1427.
[21] D. M. Guldi, N. Martin, *Carbon Nanotubes and Related Structures*, Wiley-VCH, Weinheim, Germany **2010**.
[22] T. Akasaka, F. Wudl, S. Nagase, *Chemistry of Nanocarbons*, John Wiley & Sons, Chichester, UK **2010**.
[23] M. Prato, *Nature* **2010**, *465*, 172.
[24] A. Hirsch, *Angew. Chem. Int. Ed.* **2002**, *41*, 1853.
[25] D. I. Schuster, *Nat. Chem.* **2009**, *1*, 182.
[26] C. Romero-Nieto, R. Garcia, M. A. Herranz, C. Ehli, M. Ruppert, A. Hirsch, D. M. Guldi, N. Martin, *J. Am. Chem. Soc.* **2012**, *134*, 9183.
[27] F. D'Souza, O. Ito, *Chem. Soc. Rev.* **2012**, *41*, 86.
[28] K. Dirian, M. A. Herranz, G. Katsukis, J. Malig, L. Rodriguez-Perez, C. Romero-Nieto, V. Strauss, N. Martin, D. M. Guldi, *Chem. Sci.* **2013**, *4*, 4335.
[29] F. D'Souza, R. Chitta, A. S. D. Sandanayaka, N. K. Subbaiyan, L. D'Souza, Y. Araki, O. Ito, *J. Am. Chem. Soc.* **2007**, *129*, 15865.
[30] U. Hahn, S. Engmann, C. Oelsner, C. Ehli, D. M. Guldi, T. Torres, *J. Am. Chem. Soc.* **2010**, *132*, 6392.
[31] H. Li, T. J. Jensen, F. R. Fronczek, M. G. H. Vicente, *J. Med. Chem.* **2008**, *51*, 502.
[32] M. Murata, Y. Murata, K. Komatsu, *Organic Nanomaterials: Synthesis, Characterization, and Device Applications* (Eds: T. Torres, G. Bottari), John Wiley & Sons, Hoboken, NJ, USA **2013**, p. 225.
[33] T. Nyokong, *Coord. Chem. Rev.* **2007**, *251*, 1707.
[34] A. Gouloumis, S. G. Liu, A. Sastre, P. Vazquez, L. Echegoyen, T. Torres, *Chem. Eur. J.* **2000**, *6*, 3600.
[35] J. Bartelmess, C. Ehli, J.-J. Cid, M. García-Iglesias, P. Vázquez, T. Torres, D. M. Guldi, *Chem. Sci.* **2011**, *2*, 652.
[36] J. Bartelmess, B. Ballesteros, G. de la Torre, D. Kiessling, S. Campidelli, M. Prato, T. Torres, D. M. Guldi, *J. Am. Chem. Soc.* **2010**, *132*, 16202.
[37] S. M. Bachilo, M. S. Strano, C. Kittrell, R. H. Hauge, R. E. Smalley, R. B. Weisman, *Science* **2002**, *298*, 2361.
[38] R. Graupner, *J. Raman Spectrosc.* **2007**, *38*, 673.
[39] M. S. Dresselhaus, G. Dresselhaus, A. Jorio, A. G. S. Filho, M. A. Pimenta, R. Saito, *Acc. Chem. Res.* **2002**, *35*, 1070.
[40] S. Lefrant, I. Baltog, M. Baibarac, *Synth. Met.* **2009**, *159*, 2173.